

# Potential removal of arsenite from contaminated water using a fixed bed column packed with TiO<sub>2</sub>-impregnated pomegranate peel powder

Bhoj Raj Poudel<sup>1,3</sup>, Ram Lochan Aryal<sup>2</sup>, Kedar Nath Ghimire<sup>3</sup>, Hari Paudyal<sup>3,\*</sup>  
Megh Raj Pokhrel<sup>3</sup>

<sup>1</sup>Department of Chemistry, Tri-Chandra Multiple Campus, T. U., Kathmandu, Nepal

<sup>2</sup>Department of Chemistry, Amrit Campus, Tribhuvan University, Kathmandu, Nepal

<sup>3</sup>Central Department of Chemistry, Tribhuvan University, Kathmandu, Nepal

\*Corresponding author. Email: [haripaudyal9@gmail.com](mailto:haripaudyal9@gmail.com)

## Abstract

*A dynamic biosorption of arsenite in a fixed bed column packed with TiO<sub>2</sub> impregnated pomegranate peel (PP@TiO<sub>2</sub>) has been investigated in this work, which is important to identify the effectiveness and affordability of an adsorbent in actual practice. To create an active adsorption site for As (III) ions, pomegranate peel powder (PP) was impregnated with TiO<sub>2</sub>. Under various operating parameters, the performance of a column packed with PP@TiO<sub>2</sub> for adsorbing As (III) ions was evaluated. Breakthrough curve modelling showed that the bed depth service time (BDST) and Thomas models agreed well with the experimental data. The maximum column capacity of PP@TiO<sub>2</sub> using the Thomas model was found to have resembled experimental value with high values of coefficient of determination. Therefore from these results, we may anticipate that PP@TiO<sub>2</sub> can be a strong contender for the treatment of wastewater that has traces amount of the As (III) ion in a fixed bed system.*

## Keywords

Pomegranate peel; Removal; PP@TiO<sub>2</sub>; As(III); Fixed bed column.

## Article information

Manuscript received: November 20, 2023; Revised: December 20, 2023; Accepted: December 25, 2023

DOI <https://doi.org/10.3126/bibechana.v21i1.60048>

This work is licensed under the Creative Commons CC BY-NC License. <https://creativecommons.org/licenses/by-nc/4.0/>

## 1 Introduction

Arsenic contamination in an aquatic environment has caused risk to aquatic plants and animals, and serious hazardous effects to humans even in very low concentrations [1, 2]. It can exist in several various oxidation states in aquatic environments, but the main states are As (III) and As (V) [3]. Arsenic is entered into groundwater not only by natural processes such as volcanic eruptions, dissolution of minerals ore, geochemical reaction, biological activities, etc., but also via anthropogenic sources such as wood preservatives, industrial effluents of metal processing, semiconductor, electroplating, mining, battery, pigments, dyestuff, and paints [4, 5]. Additionally, acid mine drainage wastewater contains a significant amount of arsenic [6]. Studies reported that long-term exposure to arsenic concentrations above 100 ppb may cause Blackfoot disease, hyperkeratosis, and cancers [7]. Its contamination in food and water is the main way that humans are exposed to it. The maximum permitted limit (MCL) of 10 ppb for arsenic in drinking water has been established by the USEPA and WHO because of its exposure concern and severe noxiousness [8–10]. As a result, effective and affordable arsenic removal techniques from polluted water are of emerging concern.

Conventional methods for the elimination of pollutants from contaminated water are ion exchange, electrocoagulation/co-precipitation, lime softening, reverse osmosis, ultrafiltration, nanofiltration, and resin chelation [6]. Nevertheless, most approaches have practical drawbacks, including high costs, insufficient metal removal, the production and disposal of hazardous metal sludge, and unsuitability for water with traces of contaminants [11]. Currently, adsorption is the most effective process for the removal of contaminants from water compared to other methods due to its simplicity, cost-effectiveness with high efficiency, potential for regeneration, and sludge-free operation [12]. Recently, various low-cost non-conventional adsorbents have been utilized to sequester arsenic from contaminated water [2, 3, 13–17]. To date, most of the research on the adsorption of arsenic from aqueous solutions has been done in batch mode experiments. A sorbent utilized in this study is TiO<sub>2</sub>-impregnated pomegranate peel, abbreviated as PP@TiO<sub>2</sub> hereafter. In our previous work, we focused on the As(III) removal using PP@TiO<sub>2</sub> as an adsorbent and photocatalyst using batch mode experiment [4]. The PP@TiO<sub>2</sub> was proven to be an effective, ecological, profitable, and reusable biosorbent for sequestering arsenic from contaminated water. It was also observed that the adsorbed As(III) was partly oxidized to As(V) on the adsorbent's surface. The efficient application of biomass-based adsorbents for removing As(III) in continu-

ous flow fixed-bed column adsorption systems is not well documented [18–20]. Therefore, careful attention to these details is needed to design the practical implementation of this investigated PP@TiO<sub>2</sub> and the design of industrial columns. For an industrial application or real wastewater refining, biosorption in a fixed-bed column packed with adsorbent is desirable [21–25]. Thus, the laboratory size fixed-bed column's experimental findings justify the design of an adsorption column for industrial use.

As an extension of our earlier study [4], this work extensively investigated the effectiveness of PP@TiO<sub>2</sub> in As(III) removal in a fixed-bed column mode. The biosorption capacity of SPP@TiO<sub>2</sub> for As(III) concerning some operating variables like flow rate, influent concentration, and bed depth was assessed. Experimental data were used in a variety of models, including the Yoon Nelson, Bed Depth Service Time (BDST), and Thomas models, to assess design parameters.

## 2 Materials and Methods

### 2.1 Chemicals and instruments

Analytical grade chemicals were utilized without further purification in the present work. The flow of the feed solution is controlled by using a peristaltic pump (EYELA MP-1000-MP-1000-H, Japan), whereas that of effluent samples was collected each hour using a fraction collector (Advantec SF-2120, Advantec Tokyo Kaish, Ltd., Japan).

### 2.2 Synthesis of the adsorbent (PP@TiO<sub>2</sub>)

The local juice trader in Kathmandu, Nepal, graciously provided the pomegranate peel waste. First, distilled water was used to thoroughly wash the pomegranate peels. It was then dried for 48 h at 343 to 353 K in an oven. The dry bulk was crushed and put through a copper sieve with a mesh size of 150 microns.

The biopolymer's hydroxyl groups were cross-linked by a condensation reaction using Conc. H<sub>2</sub>SO<sub>4</sub> as a dehydrating agent, preventing the adsorbent from dissolving in aqueous solutions. The cross-linked pomegranate peels were made according to Paudyal et al. (2017). In a round bottom flask, 15 g of raw peel powder was combined with 30 mL of Conc. H<sub>2</sub>SO<sub>4</sub>, which was then heated to 100°C and stirred for 24 h before cooling to room temperature.

After being neutralized with sodium bicarbonate, the charred mass was once again stirred in 1 M HCl solution. It was rinsed repeatedly in distilled water until it reached neutrality, and then it was dried at 70°C in a convection oven. The term PP refers to the powder made from pomegranate peels in this manner.

Then, PP@TiO<sub>2</sub> was prepared using a modified sol-gel method. About 10 mL of titanium (IV) n-butoxide was mixed with 15 mL of ethanol. After stirring for 30 min at room temperature, 2 g of powdered PP was added to it. Then, 15 mL of a solution of 1:1:1 ethanol, deionized water, and acetic acid were added dropwise from the burette to the magnetically stirred mixture. The whole content was further stirred for 4h until sol was obtained. The sol was dried overnight at 80°C after aging at 40°C for 2 h.

Finally, the dried gel was ground into a powder and calcined at 400°C in a muffle furnace. The resulting PP@TiO<sub>2</sub> was stored in a plastic container before being used in the characterization and adsorption experiment. The detailed methodology for preparing PP@TiO<sub>2</sub> is shown in Scheme 1.

### 2.3 Characterization

As a continuation of our previous study, the methodology and results of the characterization of PP@TiO<sub>2</sub> before and after adsorption have been described in detail elsewhere [4].

In brief, EDX spectra showed peaks associated with Ti after TiO<sub>2</sub> impregnation (PP@TiO<sub>2</sub>), indicating that the biomass had been effectively impregnated with TiO<sub>2</sub>. The EDX spectra of As(III) adsorbed PP@TiO<sub>2</sub> showed an additional peak associated with arsenic. This demonstrated that arsenic had been effectively adsorbed from an aqueous solution by PP@TiO<sub>2</sub>.

In XRD analysis, the diffraction peaks associated with crystalline TiO<sub>2</sub> in the case of PP@TiO<sub>2</sub> emerge at  $2\theta = 25.2^\circ, 38.1^\circ, 48^\circ, 55^\circ, 63^\circ, 70^\circ, \text{ and } 75^\circ$ . The (1 0 1), (0 0 4), (2 0 0), (1 0 5), (2 0 4), (2 2 0), and (2 1 5) planes, respectively, are represented by these peaks. This demonstrates that TiO<sub>2</sub> was successfully embedded in biomass in the form of crystalline anatase. These peaks demonstrate excellent agreement with JCPDS card No. 00-021-1272 of the TiO<sub>2</sub> anatase phase.

In FTIR spectra of PP@TiO<sub>2</sub>, the Ti-O vibration, which represents the contact of TiO<sub>2</sub> with PP, is attributed to absorption peaks between 420 and 700 cm<sup>-1</sup>. This offers convincing proof of TiO<sub>2</sub> impregnation with the creation of the Ti-O-C bond. In the FTIR spectra of As(III) adsorbed PP@TiO<sub>2</sub>, an extra peak related to As-O vibrations was discovered at 825 cm<sup>-1</sup> following arsenic biosorption. This supports the biosorption of As(III) onto PP@TiO<sub>2</sub>.

Using SEM coupled with an EDX spectrometer, the morphology and elemental composition of as-synthesized biosorbent were examined. The crystallinity of the PP@TiO<sub>2</sub> was determined using XRD patterns from an X-ray diffractometer. Using FTIR spectroscopy, the surface functional-

ities of the biosorbents before and after biosorption of As(III) were examined. The XPS investigations were performed by using an XPS spectrometer (Thermo Fisher Scientific, UK) to identify the elemental bonding and chemical states.

### 2.4 Dynamic adsorption test in fix bed column

As seen in Figure 1, a glass column with an inner diameter of 0.8 cm and a height of 20 cm was used for the continuous adsorption test of As(III) in a fixed bed column. For this, the PP@TiO<sub>2</sub> was soaked in DI water before being packed into the column. Following that, the wet adsorbent was packed into a column. The column was first filled with glass beads (5 cm), then with a layer of cotton (2 cm), and then PP@TiO<sub>2</sub> (1.4 to 4.1 cm). The column was once more packed with a 2 cm cotton layer trailed by a 5 cm glass bead layer.

Before the biosorption test, the column was conditioned by passing DI water for 5 h at the same pH as the test solution. After this, As(III) solution (10 mg/L) was passed into the column at the required flow rate by using a peristaltic pump. The effluent solutions for the measurement were collected at each regular interval with the help of a fraction collector. Alkali solution (0.1 M NaOH) was used to elute the loaded As(III) since they had been successfully used in earlier batch tests. The effluent samples were then analyzed to measure the final concentrations of arsenic by using ICP-MS.

### 2.5 Analysis of breakthrough curve parameters

It is crucial to study the breakthrough curve to evaluate a column's biosorption performance. Calculating the breakthrough curve parameters can do this. The ratio of As(III) concentration from the effluent to the intake,  $\frac{C_e}{C_i}$ , is presented against time ( $h$ ) following the commencement of the flow. Equation 1 provides the total quantity of adsorbate ion sorbed onto the packed column,  $q_{total}$ , and the dynamic biosorption capacity,  $q_e$  [21, 23].

$$q_{total} = \frac{QA}{1000} = \frac{Q}{1000} \int_{t=0}^{t=total} C_{ads} dt \quad (1)$$

$$q_e = \frac{q_{total}}{M} \quad (2)$$

where  $t_{total}$ ,  $Q$ ,  $A$ ,  $M$ , and  $C_{ads}$  stand for, respectively, the total flow period for the column to grasp exhaustion, volumetric flow rate, the area under the breakthrough curve, the quantity of biosorbent (g), the difference in the initial and the effluent adsorbate concentration. Equation 3 may be used to determine the mass transfer zone [26]:

$$MTZ = Z \frac{t_E - t_B}{t_E} \quad (3)$$

where  $Z$  denotes the bed height (cm);  $t_B$  denotes the breakthrough time, and  $t_E$  is the exhaustion duration.

### 2.6 Breakthrough curve modeling

The breakthrough curve must be predicted to design and optimize the column for the biosorption process. For this, three mathematical models: the Yoon-Nelson model, and the Bed depth service time (BDST) model, were employed in this work to examine the dynamic biosorption efficiency of PP@TiO<sub>2</sub>. The column experiment conditions are presented in Table 1.

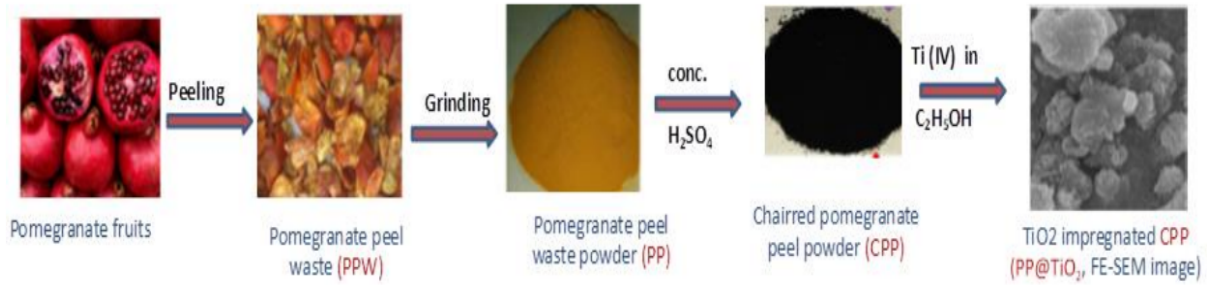
#### 2.6.1 Thomas model

This model assumes that mass transfer at the interface rather than chemical interactions restricts

adsorption, and experimental results exhibit Langmuir isotherms and second-order kinetics [27]. This is appropriate for illustrating the entire breakthrough curve [26]. The following Equation 4 may be used to express the Thomas model in linear form [21, 28]:

$$\ln \left( \frac{C_i}{C_e} - 1 \right) = k_{Th} \frac{q_0 M}{Q} = k_{Th} C_i t \quad (4)$$

where  $k_{Th}$  denotes Thomas rate constant (mL/min.mg),  $q_e$  represents the equilibrium biosorption capacity (mg/g),  $M$  represents the mass of biosorbent (g), and  $Q$  denotes the feed rate (mL/min). The linear plot of  $\ln (C_i/C_e - 1)$  vs  $t$  allowed for the evaluation of the values  $k_{Th}$  and  $q_e$ .



**Scheme 1:** Flowsheet detailing the synthesis of PP@TiO<sub>2</sub> from biomass derived from pomegranate peels.

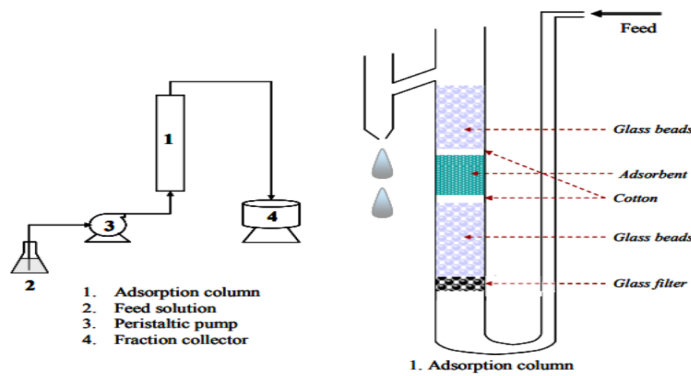


**Figure 1:** Schematic diagram for the column experiments (Figure adapted with permission from Biswas et al. 2008 [25], Copyright, Elsevier).

**Table 1.** Experimental conditions for column tests

<b>Influence of flow rate:</b>	
pH	7.0
Adsorbent mass	0.86 g
Initial As(III) concentration	10.0 mg/L
Bed height	4.1 cm
Bed volume	2.06 cm <sup>3</sup>
<i>Variable conditions</i>	
Flow rate	72, 150, 240 mL/h
<b>Effect of initial As(III) concentration:</b>	
Bed height	4.1 cm
Adsorbent mass	0.86 g
Flow rate	150 mL/h
Bed volume	2.06 cm <sup>3</sup>
pH	7.0
<i>Variable conditions</i>	
Initial As(III) concentration	5.0, 10.0, 15.0 mg/L
<b>Effect of bed height:</b>	
Flow rate	60 mL/h
Initial As(III) concentration	10 mg/L
pH	7.0
<i>Variable conditions</i>	
Bed height	1.4, 2.6, 4.1 cm
Adsorbent mass	0.31 g for 1.4 cm, 0.55 g for 2.6 cm and 0.86 g for 4.1 cm

### 2.6.2 Yoon-Nelson model

This model presumes that the probability of biosorption for each adsorbate ion decreases at a rate that is proportionate to its probability of both biosorption and breakthrough of biosorbent from the biosorbent [29]. In the later phases of the breakthrough curve, the Yoon-Nelson model, like the Thomas model, may reduce the shortcomings of the Adams-Bohart model. The Yoon-Nelson model's linear expression is presented by the following Equation 5 [23, 30]:

$$\ln\left(\frac{C_e}{C_i - C_e}\right) = k_{YN} - \tau k_{YN} \quad (5)$$

where  $\tau$  denotes the amount of time required for a 50% adsorbate breakthrough in minutes and  $k_{YN}$  denotes the Yoon-Nelson rate constant ( $\text{min}^{-1}$ ).

### 2.6.3 Bed depth service time (BDST) model

This model predicts that bed depth and service time will be linearly related for a certain breakthrough concentration. Past studies state that this model does a good job of explaining the first 10 to 50% of the breakthrough curve [7]. Equation 6 provides the linear expression of the BDST model [21]:

$$t_B = \frac{N_0 Z}{C_i U_0} - \frac{1}{k_b C_i} \ln\left(\frac{C_i}{C_b} - 1\right) \quad (6)$$

where  $N_0$  is the column adsorption capacity ( $\text{mg/L}$ ),  $t_B$  denotes the service period of column (in hours),  $C_b$  denotes the outflow concentration at breakthrough point ( $\text{mg/L}$ ), and  $k_b$  denotes the rate constant [ $\text{L}/(\text{mg}\cdot\text{h})$ ]. The BDST parameters,  $N_0$ , and  $k_b$ , are computed from the time versus bed depth graphs.

### 2.6.4 Adams Bohrt model

This model works better in situations where the effluent concentration is lower. Adams-Bohrts model predicts that the biosorption rate is proportional to the biosorbent concentration and the residual capacity of the solids. In the linear form, it can be written as [31],

$$\ln\left(\frac{C_t}{C_i}\right) = k_{AB} C_i \times -\frac{N_0}{U_0} k_{AB} Z \quad (7)$$

where  $C_i$  is the initial concentration ( $\text{mg/L}$ ) of As(V);  $C_t$  is the concentration ( $\text{mmol/L}$ ) of As(V) at time  $t$ ;  $k_{AB}$  is the Bohart-Adams model rate constant ( $\text{L}/\text{min}$ );  $N_0$  is the column saturation concentration ( $\text{mg/L}$ );  $Z$  is the height of the bed (cm) in a column.

## 3 Results and Discussion

### 3.1 Characterization

As a continuation of our previous study, the adsorbents used in this study were thoroughly char-

acterized in previous research [4]. Their relevant characteristics are briefly mentioned here.

### 3.1.1 EDX spectra adsorbent before and after As(III) adsorption

The EDX spectra of PP, PP@TiO<sub>2</sub>, and As(III) adsorbed PP@TiO<sub>2</sub> are revealed in Figure 2(a), Figure 2(b), and Figure 2(c), correspondingly. The EDX spectra showed peaks associated with Ti after TiO<sub>2</sub> impregnation (PP@TiO<sub>2</sub>), indicating that the biomass had been effectively impregnated with TiO<sub>2</sub>. The EDX spectra of As(III) adsorbed PP@TiO<sub>2</sub> showed an additional peak associated with arsenic. This demonstrated that arsenic had been effectively adsorbable from an aqueous solution by PP@TiO<sub>2</sub>.

### 3.1.2 XRD pattern of biosorbent

Figure 3 displays the XRD pattern of PP and PP@TiO<sub>2</sub>. The absence of sharp peaks in the PP signals its amorphous nature. The diffraction peaks associated with crystalline TiO<sub>2</sub> in the case of PP@TiO<sub>2</sub> emerge at  $2\theta = 25.2^\circ, 38.1^\circ, 48^\circ, 55^\circ, 63^\circ, 70^\circ, \text{ and } 75^\circ$ . The (1 0 1), (0 0 4), (2 0 0), (1 0 5), (2 0 4), (2 2 0), and (2 1 5) planes, respectively, are represented by these peaks. This demonstrates that TiO<sub>2</sub> was successfully embedded in biomass in the form of crystalline anatase. These peaks demonstrate excellent agreement with JCPDS card No. 00-021-1272 of the TiO<sub>2</sub> anatase phase.

### 3.1.3 Functional group analysis

FTIR spectra were used to confirm the functional groups on the biosorbents, as given in Figure 4. In the FTIR spectra of PP@TiO<sub>2</sub>, the Ti-O vibration, which represents the contact of TiO<sub>2</sub> with PP, is attributed to absorption peaks between 420 and 700 cm<sup>-1</sup>. This offers convincing proof of TiO<sub>2</sub> impregnation with the creation of the Ti-O-C bond. In the

FTIR spectra of As(III) adsorbed PP@TiO<sub>2</sub>, an extra peak related to As-O vibrations was discovered at 825 cm<sup>-1</sup> following arsenic biosorption. This supports the biosorption of As(III) onto PP@TiO<sub>2</sub>.

### 3.2 Effect of the flow rate

The impact of the flow rate of the inflowing solution on the As(III) biosorption by PP@TiO<sub>2</sub> was investigated at different flow rates (72, 150, and 240 mL/h) and a fixed bed height (4.1 cm), and preliminary As(III) concentration (10.0 mg/L). The breakthrough data presented in Figure 5(a) indicates that a lesser time is sufficient for column breakthrough, whereas its value is increased with the decrease of flow rate. This is attributed to the possibility of channeling and short contact between the As(III) ions and active sites of PP@TiO<sub>2</sub> bed at a higher flow rate. Moreover, the treated bed volumes are determined to be 297.1, 327.7, and 349.5 at flow rates of 72, 150, and 240 mL/h, respectively. Another reason for an earlier breakthrough might be because a greater volume of solution containing a greater number of As(III) ions passed across the bed at a higher flow rate. Consequently, more As(III) ions became in contact with the adsorbent sites of PP@TiO<sub>2</sub>, making them get saturated more rapidly.

Likewise, a higher biosorption capacity is achieved at a lower flow rate as expected. As the flow rate increased, the amount of As(III) passed through the PP@TiO<sub>2</sub> bed containing a fixed number of active sites increased; however, the contact time between the adsorbate and adsorbent potentially reduced, which increases the possibility of channeling. Because of this, the limited number of active sites are colloids or adsorbed with As(III) ion resulting in a decrease in column adsorption capacity. The longer contact time and lesser channeling led to more efficient adsorption of As(III) onto PP@TiO<sub>2</sub>, and thus, a higher biosorption capacity was attained at a lower flow rate.

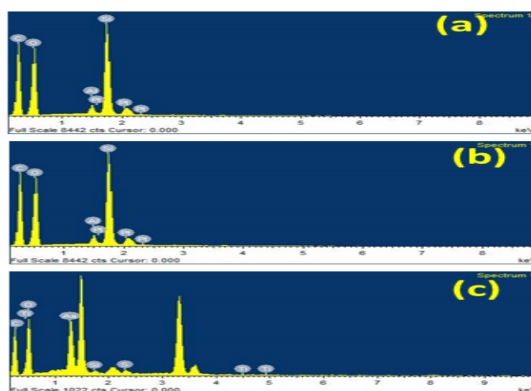


Figure 2: EDX spectra of (a) PP, (b) PP@TiO<sub>2</sub> and (c) As(III) adsorbed PP@TiO<sub>2</sub>.

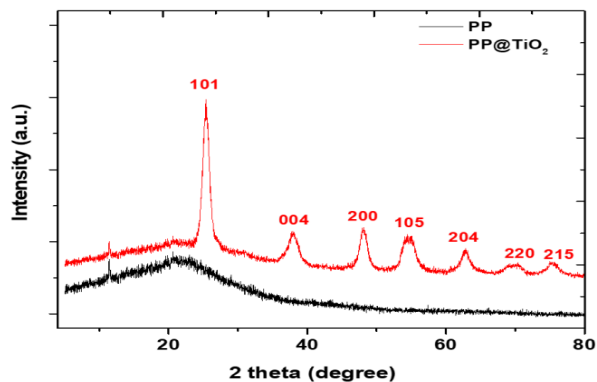


Figure 3: XRD spectra of PP and PP@TiO<sub>2</sub>.

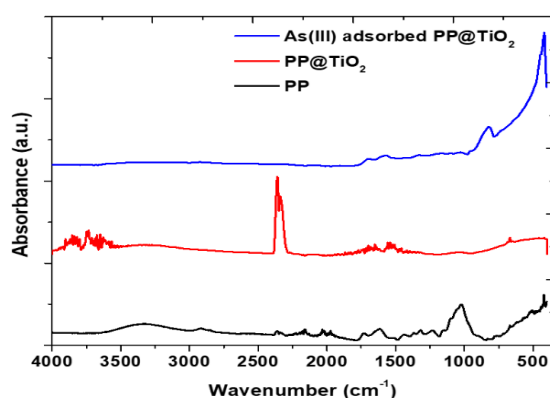


Figure 4: FTIR spectra of PP, PP@TiO<sub>2</sub> and As(III) adsorbed PP@TiO<sub>2</sub>.

### 3.3 Effect of initial As(III) concentration

The breakthrough curves at varying initial As(III) concentrations for a flow rate of 150 mL/h and a bed height of 4.1 cm are shown in Figure 6(a). The treated bed volumes were 436.9, 327.7, and 145.63 for initial As(III) concentrations of 5.0, 10.0, and 15.0 mg/L, respectively. The figure clearly shows that with increasing initial As(III) concentration, the biosorption approached saturation more quickly, and the breakthrough time was decreased. A similar trend was reported by Paudyal et al., 2013 [21]. The decrease in breakthrough time at higher concentrations is due to the contact of a large number of As(III) at high concentrations of arsenic with active sites in the PP@TiO<sub>2</sub> bed.

The biosorption capacity of PP@TiO<sub>2</sub> for As(III) also increased (2.31 to 3.14 mg/g) with increasing initial As(III) concentration, which can probably be attributed to the higher concentration offering more driving force for the transfer process.

### 3.4 Effect of bed height

Figure 7(a) depicted the impact of bed height on the breakthrough curves regarding As(III) biosorption onto the PP@TiO<sub>2</sub>. The treated bed volumes

of As(III) solution increased from 515.5 to 625.0, and 687.8 with an increasing bed height of 1.4, 2.6, and 4.1 cm, respectively, which may relate to an extended contact duration. The evaluated As(III) removal capacity of PP@TiO<sub>2</sub> for the bed heights of 4.1, 2.6, and 1.4 cm are presented in Table 2.

### 3.5 Modeling of the breakthrough curve

This study explores the dynamic biosorption behavior of PP@TiO<sub>2</sub> using the Thomas, Yoon-Nelson, and Adams-Bohart models. Figures 5(b), 5(c), and 5(d), respectively, show the modeling curve of Thomas, Yoon-Nelson, and Adams-Bohart models at different flow rates. Figures 6(b), 6(c), and 6(d), respectively, show the modeling curve of Thomas, Yoon-Nelson, and Adams-Bohart models at different As(III) concentrations. Similarly, Figures 7(b), 7(c), and 7(d), respectively, show the modeling curve of Thomas, Yoon-Nelson, and Adams-Bohart models at different bed heights. Table 2 shows the results or dynamic parameters obtained for the adsorption of As(III) onto the column of PP@TiO<sub>2</sub> using various models.

The entire breakthrough curve may be analyzed using the Thomas model. This model presupposes

that mass transfer at the interface limits biosorption and that the data follows second-order kinetics and Langmuir isotherms. The dynamic biosorption capacity rose from 3.81 to 2.86 mg/g as the flow rate increased from 72 to 240 mL/h, whereas the Thomas rate constant increased from 0.127 to 0.521 L/mg·h. In a packed bed system, homogeneous contact decreases due to channeling, which causes  $q_0$  to decline at greater flow rates. The Thomas rate constant increased from 0.1992 to 0.2567 L/mg·h, and the biosorption capacity increased from 2.31 to 3.13 mg/g as the initial As(III) concentration rose from 5.0 to 15.0 mg/L. The higher concentration gradient provided a greater driving force, and a higher amount of mass transfer occurred through the adsorbent bed, causing better biosorption capacity at the higher concentration of As(III). Similar results were observed by Paudyal et al., 2013, in the case of fluoride adsorption using Zr(IV) modified dried orange juice residue [21].

In the case of the Yoon-Nelson model, it was discovered that, with an increase in flow rate from 72 to 240 mL/h,  $k_{YN}$  rose from 1.271 to 2.961 h<sup>-1</sup>,

and  $\tau$  reduced from 4.54 to 1.04 h, respectively. The  $k_{YN}$  values fall from 1.194 to 0.047 h<sup>-1</sup> when the bed height rises from 1.4 to 4.1 cm, while  $\tau$  increases from 89.3 to 165.1 h. An increase in the  $k_{YN}$  values from 0.996 to 5.472 h<sup>-1</sup> and a drop in  $\tau$  from 4.63 to 1.04 h was brought on by a change in the initial As(III) concentration from 5 to 15 mg/L.

The Adams-Bohart model, which is used to evaluate the initial part of the breakthrough curve ( $C_t/C_0 = 0$  to 0.5), assumes that equilibrium is not instantaneous. When the initial As(III) concentration was increased from 5 to 10 mg/L, the kinetic constant  $k_{AB}$  reduced from 0.175 to 0.042 L/mg·h, but it rose when the flow rate was increased from 72 to 240 mL/h from 0.063 to 0.181 L/mg·h. Additionally, a rise in bed height from 1.4 to 4.1 cm caused  $k_{AB}$  to fall from 0.0725 to 0.0552 L/mg·h. With an increase in flow rate from 72 to 240 mL/h, the column saturation concentration of the adsorbent ( $N_0$ ) decreased from 2532 to 2195 mg/L, respectively. When the initial As(III) concentration was increased from 5 to 15 mg/L,  $N_0$  values increased from 1.63 to 7.91 mg/L, respectively.

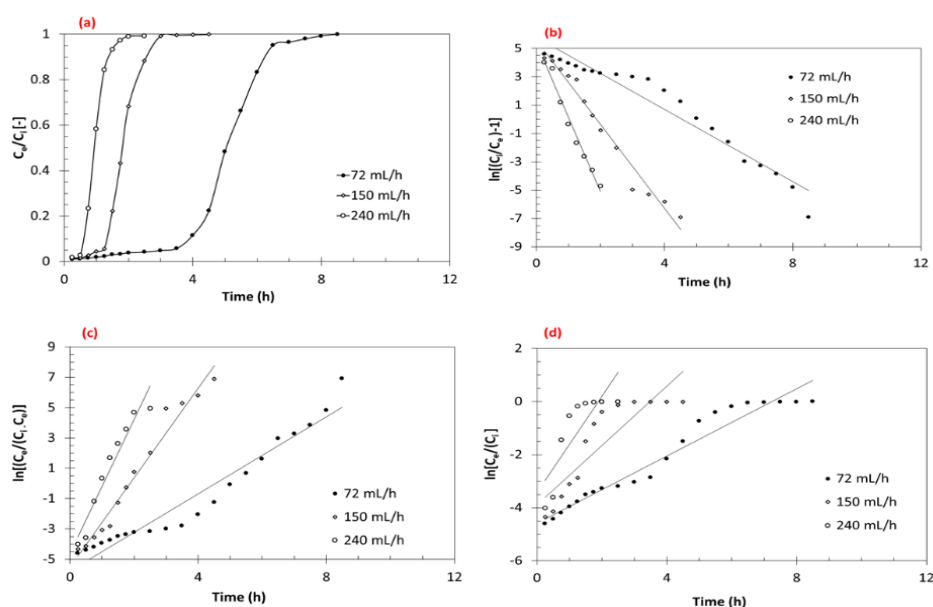


Figure 5: Biosorption of As(III) onto PP@TiO<sub>2</sub> in fixed bed system at different flow rates (a) breakthrough profile, and modeling using (b) Thomas, (c) Yoon Nelson, and (d) Adams-Bohrats models.

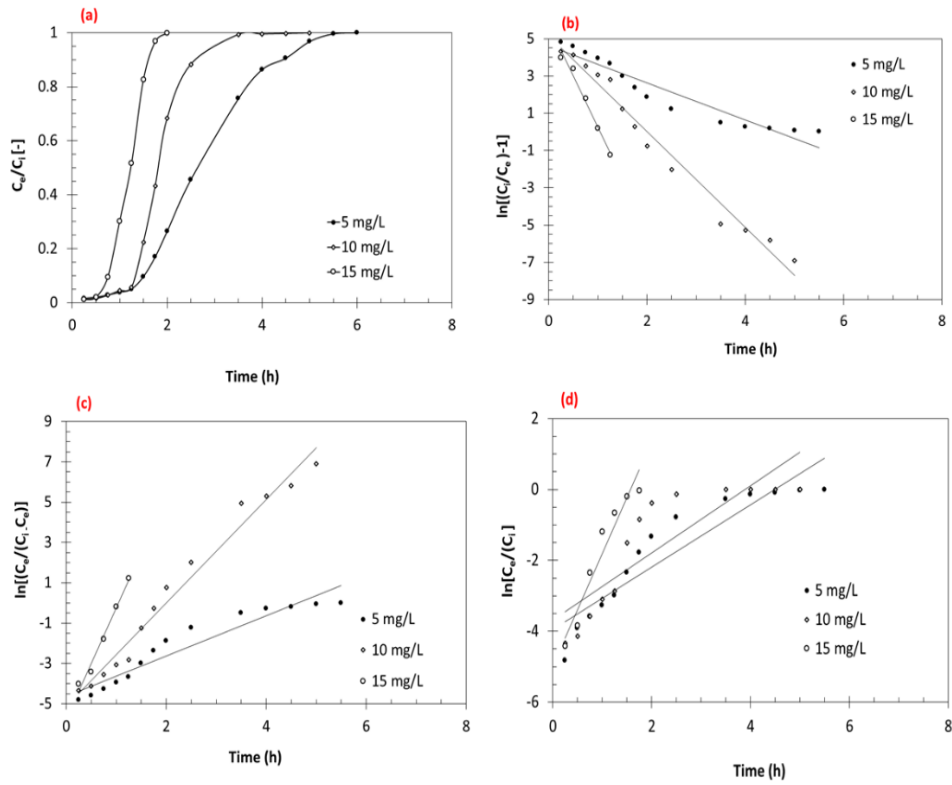


Figure 6: Biosorption of As(III) onto PP@TiO<sub>2</sub> in fixed bed system at different concentrations (a) breakthrough profile, and modeling using (b) Thomas, (c) Yoon Nelson, and (d) Adams-Bohrats models.

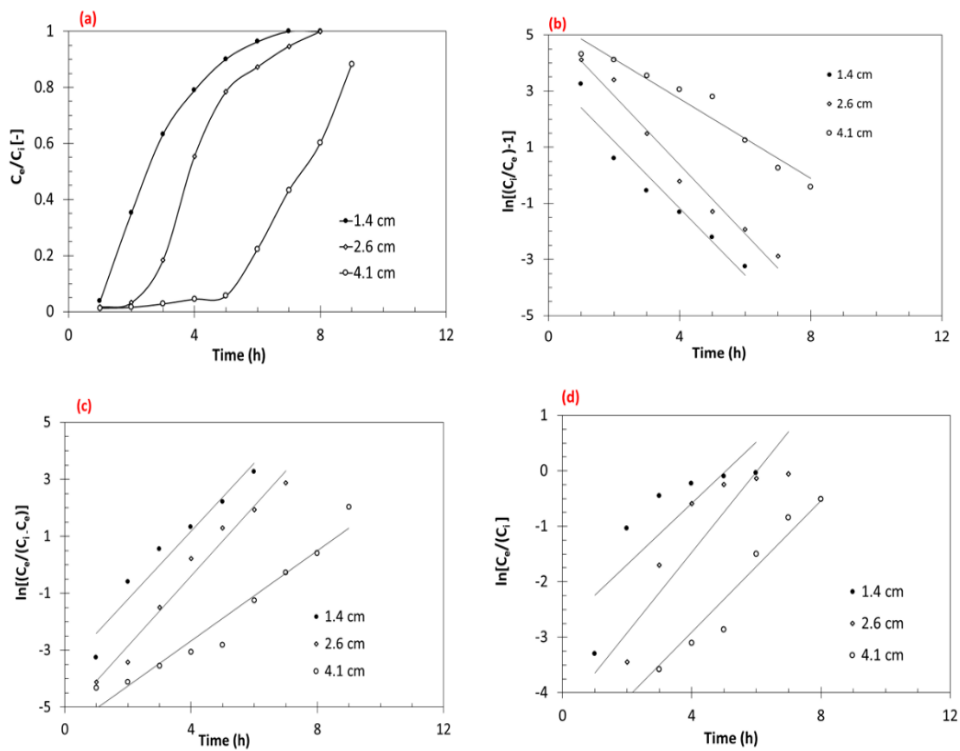


Figure 7: Biosorption of As(III) onto PP@TiO<sub>2</sub> in fixed bed system at different bed height (a) breakthrough profile, and modeling using (b) Thomas, (c) Yoon Nelson, and (d) Adams-Bohrats models.

**Table 2.** Parameters of various models for the adsorption of As(III) in the fixed bed column of PP@TiO<sub>2</sub>.

Experimental parameters				Thomas parameters			Yoon Nelson parameters			Adams-Bohart parameters		
F (mL/h)	C <sub>i</sub> (mg/L)	Z (cm)	q <sub>exp</sub> (mg/g)	q <sub>0</sub> (mg/g)	k <sub>Th</sub> (L/mg h)	R <sup>2</sup>	τ (h)	K <sub>YN</sub> (1/h)	R <sup>2</sup>	N <sub>0</sub> (mg/L)	K <sub>AB</sub> (L/mg h)	R <sup>2</sup>
72	10	4.1	4.06	3.81	0.13	0.94	4.54	1.27	0.94	2532	0.063	0.95
150	10	4.1	3.57	3.28	0.29	0.97	1.87	2.96	0.97	2529	0.112	0.78
240	10	4.1	3.07	2.86	0.52	0.98	1.04	4.44	0.93	2195	0.18	0.68
150	5	4.1	2.31	4.04	0.19	0.94	4.63	0.99	0.91	1.63	0.17	0.85
150	10	4.1	2.79	3.49	0.25	0.97	2.00	2.56	0.97	2.83	0.09	0.74
150	15	4.1	3.13	2.74	0.36	0.98	1.04	5.47	0.98	7.91	0.04	0.95
60	10	1.4	10.58	11.59	0.14	0.94	3.01	1.19	0.94	10798	0.07	0.69
60	10	2.6	12.40	11.76	0.10	0.97	4.31	1.23	0.97	6924	0.05	0.86
60	10	4.1	13.58	14.59	0.09	0.95	6.76	0.05	0.94	6780	0.05	0.96

#### 4 Conclusion

The results of this research show that the novel adsorbent, PP@TiO<sub>2</sub>, is successful in removing As(III) from water utilizing a fixed bed column. The flow rate, initial As (III) concentration, and bed depth all had an impact on how well As (III) could be absorbed via a fixed-bed column. It was discovered that the design parameters may be accurately predicted using the Thomas and the BDST model. To remove As (III) from wastewater, it is anticipated that the PP@TiO<sub>2</sub> will be a good choice.

#### Acknowledgments

The first author (B.R. Poudel) acknowledges funding support from Ph.D. Research Grant (Grant No. 2078), Office of the Rector, Research Directorate, Tribhuvan University, Kathmandu, Nepal.

#### References

- [1] B.R. Poudel, R.L. Aryal, S.K. Gautam, K.N. Ghimire, H. Paudyal, and M.R. Pokhrel. Effective remediation of arsenate from contaminated water by zirconium modified pomegranate peel as an anion exchanger. *J. Environ. Chem. Eng.*, 9:106552, 2021.
- [2] M.B. Shakoore, N.K. Niazi, I. Bibi, M. Shahid, F. Sharif, S. Bashir, S.M. Shaheen, H. Wang, D.C. Tsang, and Y.S. Ok. Arsenic removal by natural and chemically modified water melon rind in aqueous solutions and groundwater. *Sci. Total Environ.*, 645:1444–1455, 2018.
- [3] K.N. Ghimire, K. Inoue, H. Yamaguchi, K. Makino, and T. Miyajima. Adsorptive separation of arsenate and arsenite anions from aqueous medium by using orange waste. *Water Res.*, 37:4945–4953, 2003. <https://doi.org/10.1016/j.watres.2003.08.029>
- [4] B.R. Poudel, R.L. Aryal, S. Bhattarai, A.R. Koirala, S.K. Gautam, K.N. Ghimire, B. Pant, M. Park, H. Paudyal, and M.R. Pokhrel. Agro-waste derived biomass impregnated with tio2 as a potential adsorbent for removal of as (iii) from water. *Catalysts*, 10:1125, 2020. <https://doi.org/10.3390/catal10101125>
- [5] B.R. Poudel, D.S. Ale, R.L. Aryal, K.N. Ghimire, S.K. Gautam, H. Paudyal, and M.R. Pokhrel. Zirconium modified pomegranate peel for efficient removal of arsenite from water. *BIBECHANA*, 19:1–13, 2022.

<https://doi.org/10.1016/j.jece.2021.106552>

- <https://doi.org/10.3126/bibechana.v19i1-2.45943>
- [6] D. Mohan and C.U. Pittman Jr. Arsenic removal from water/wastewater using adsorbents—a critical review. *J. Hazard. Mater.*, 142:1–53, 2007. <https://doi.org/10.1016/j.jhazmat.2007.01.006>
- [7] C. Jain and I. Ali. Arsenic: occurrence, toxicity and speciation techniques. *Water Res.*, 34:4304–4312, 2000.
- [8] J.A. Cotruvo. 2017 who guidelines for drinking water quality: first addendum to the fourth edition. *J. Am. Water Works Assoc.*, 109:44–51, 2017.
- [9] World Health Organization (WHO). Arsenic in drinking-water background document for development of who guidelines for drinking-water quality. 2011. [http://www.who.int/water\\_sanitation\\_health/dwq/chemicals/arsenic.pdf](http://www.who.int/water_sanitation_health/dwq/chemicals/arsenic.pdf)
- [10] United States Environmental Protection Agency (USEPA). Drinking water requirements for states and public water system. 2017.
- [11] G. Murugesan, M. Sathishkumar, and K. Swaminathan. Arsenic removal from groundwater by pretreated waste tea fungal biomass. *Bioresour. Technol.*, 97:483–487, 2006.
- [12] N. Bashyal, S. Aryal, R. Rai, P.C. Lohani, S.K. Gautam, M.R. Pokhrel, and B.R. Poudel. Effective biosorption of phosphate from water using fe (iii)-loaded pomegranate peel. *Chem. Biochem. Eng. Q.*, 37:67–77, 2023. <https://doi.org/10.15255/CABEQ.2022.2174>
- [13] A. Gupta, S.R. Vidyarthi, and N. Sankararamkrishnan. Concurrent removal of as (iii) and as (v) using green low-cost functionalized biosorbent-saccharum officinarum bagasse. *J. Environ. Chem. Eng.*, 3:113–121, 2015. <https://doi.org/10.1016/j.jece.2014.11.023>
- [14] D. Humelnicu, L.V. Soroaga, C. Arsene, I. Humelnicu, and R.I. Olariu. Adsorptive performance of soy bran and mustard husk towards arsenic (v) ions from synthetic aqueous solutions. *Acta Chim. Slov.*, 66:326–336, 2019.
- [15] R.L. Aryal, K.P. Bhurtel, B.R. Poudel, M.R. Pokhrel, H. Paudyal, and K.N. Ghimire. Sequestration of phosphate from water onto modified watermelon waste loaded with zr (iv). *Sep. Sci. Technol.*, pages 1–13, 2021. <https://doi.org/10.1080/01496395.2021.1884878>
- [16] K.P. Bhattarai, B.D. Pant, R. Rai, R.L. Aryal, H. Paudyal, S.K. Gautam, K.N. Ghimire, M.R. Pokhrel, and B.R. Poudel. Efficient sequestration of cr (vi) from aqueous solution using biosorbent derived from arundo donax stem. *J. Chem.*, 2022:9926391, 2022. <https://doi.org/10.1155/2022/9926391>
- [17] E. Pehlivan, H. Tran, W. Ouédraogo, C. Schmidt, D. Zachmann, and M. Bahadir. Sugarcane bagasse treated with hydrous ferric oxide as a potential adsorbent for the removal of as (v) from aqueous solutions. *Food Chem.*, 138:133–138, 2013.
- [18] T.T.Q. Nguyen, P. Loganathan, T.V. Nguyen, S. Vigneswaran, and H.H. Ngo. Iron and zirconium modified luffa fibre as an effective bioadsorbent to remove arsenic from drinking water. *Chemosphere*, 258:127370, 2020. <https://doi.org/10.1016/j.chemosphere.2020.127370>
- [19] C.Y. Chen, T.H. Chang, J.T. Kuo, Y.F. Chen, and Y.C. Chung. Characteristics of molybdate-impregnated chitosan beads (micb) in terms of arsenic removal from water and the application of a micb-packed column to remove arsenic from wastewater. *Bioresour. Technol.*, 99:7487–7494, 2008.
- [20] S. Baral, N. Das, T. Ramulu, S. Sahoo, S. Das, and G.R. Chaudhury. Removal of cr (vi) by thermally activated weed salvinia cucullata in a fixed-bed column. *J. Hazard. Mater.*, 161:1427–1435, 2009.
- [21] H. Paudyal, B. Pangeni, K. Inoue, H. Kawakita, and K. Ohto. Adsorptive removal of fluoride from aqueous medium using a fixed bed column packed with zr (iv) loaded dried orange juice residue. *Bioresour. Technol.*, 146:713–720, 2013.
- [22] P. Roy, N.K. Mondal, S. Bhattacharya, B. Das, and K. Das. Removal of arsenic (iii) and arsenic (v) on chemically modified low-cost adsorbent: batch and column operations. *Appl. Water Sci.*, 3:293–309, 2013.
- [23] R. Sharma and B. Singh. Removal of ni (ii) ions from aqueous solutions using modified rice straw in a fixed bed column. *Bioresour. Technol.*, 146:519–524, 2013.

- [24] T.S. Singh and K. Pant. Experimental and modelling studies on fixed bed adsorption of as (iii) ions from aqueous solution. *Sep. and Purif. Technol.*, 48:288–296, 2006.
- [25] B.K. Biswas, J.I. Inoue, K. Inoue, K.N. Ghimire, H. Harada, K. Ohto, and H. Kawakita. Adsorptive removal of as (v) and as (iii) from water by a zr (iv)-loaded orange waste gel. *J. Hazard. Mater.*, 154:1066–1074, 2008.  
<https://doi.org/10.1016/j.jhazmat.2007.11.030>
- [26] D. Bulgariu and L. Bulgariu. Sorption of pb (ii) onto a mixture of algae waste biomass and anion exchanger resin in a packed-bed column. *Bioresour. Technol.*, 129:374–380, 2013.
- [27] K. Foo, L. Lee, and B. Hameed. Preparation of tamarind fruit seed activated carbon by microwave heating for the adsorptive treatment of landfill leachate: a laboratory column evaluation. *Bioresour. Technol.*, 133:599–605, 2013.
- [28] H.C. Thomas. Heterogeneous ion exchange in a flowing system. *J. Am. Chem. Soc.*, 66:1664–1666, 1944.
- [29] N.H. Mthombeni, S. Mbakop, A. Ochieng, and M.S. Onyango. Adsorptive removal of v (v) ions using clinoptilolite modified with polypyrrole and iron oxide nanoparticles in column studies. *MRS Adv.*, 3:2119–2127, 2018.
- [30] Y.H. Yoon and J.H. Nelson. Application of gas adsorption kinetics i. a theoretical model for respirator cartridge service life. *Am. Ind. Hyg. Assoc. J.*, 45:509–516, 1984.  
<https://doi.org/10.1080/15298668491400197>
- [31] G.S. Bohart and E.Q. Adams. Some aspects of the behavior of charcoal with respect to chlorine. *J. Am. Chem. Soc.*, 42:523–544, 1920.